Evidence for a nuclear halo from ^{11}Li elastic scattering measured at 637 MeV incident energy on a ^{12}C target

Michel C. Mermaz
Service de Physique Nucléaire, Centre d'Etudes de Saclay, 91191 Gif sur Yvette CEDEX, France
(Received 13 January 1993)

An optical model analysis of the elastic scattering of ^{11}C and ^{11}Li on ^{12}C target nuclei has been performed, for measurements at 620 and 637 MeV laboratory incident energy, respectively. The data are from the group of the University of Notre Dame. It has turned out, in the case of the ^{11}Li projectile, that it was necessary to use a real and imaginary surface potential peaked very far outside of the nucleus core, in order to reproduce the elastic scattering angular distribution at very forward angles. The extracted optical model reaction cross section leads to a radius of 3.7 fm for ^{11}Li in agreement with what is already known in the literature from interaction cross section measurements. On the contrary, the extracted radius for the ^{11}C nucleus is 2.5 fm in this experiment. Furthermore, at this high incident energy, a strong far-side component on ^{11}Li is evidenced by a Fuller analysis. This large radius for the ^{11}Li nucleus, added to the fact that strong refractive effects are observed in the elastic scattering, is a clear signature of a nuclear halo for the ^{11}Li nucleus.

PACS number(s): 25.60.+v, 25.70.−z, 25.70.Bc

I. INTRODUCTION

The arguments in favor of a halo for the ^{11}Li nucleus are twofold. First, the halo has to increase largely the reaction cross section. Second, a strong refractive effect has to be present in the elastic scattering: the cross section is far-side dominated.

Measurements of interaction cross sections on the light *p*-shell nuclei by Tanihata *et al.* [1], performed at 790 MeV/nucleon, have led to an interaction cross section for the ^{11}Li+^{12}C system of 1040±40 mb. An interaction nuclear radius of 3.14±0.16 fm follows for the ^{11}Li nucleus, compared to 2.41±0.02 fm for the ^{9}Li nucleus obtained in the same systematic study. A recent calculation by Bertsch, Brown, and Sagawa [2], based on a simplified Glauber approach with densities constrained by the empirical binding energies, predicts a slightly smaller cross section of 1000 mb due to the 0.19 MeV weak binding energy of the last neutron pair of the ^{11}Li nucleus.

Recent exploratory studies of ^{11}Li elastic scattering from a ^{12}C target by Satchler, McVoy, and Hussein [3] predict a clear far-side domination of the elastic-scattering cross section due to the two-neutron halo of the ^{11}Li nucleus. This halo has also to increase dramatically the reaction cross section up to, for instance, 1500 mb at 85 MeV/nucleon incident energy.

The optical-model analysis of elastic scatterings of ^{11}Li and ^{11}C on a ^{12}C target performed by Kolata *et al.* [4] on their own data taken at 637 and 620 MeV laboratory incident energy, respectively, indicates a strong refractive effect for the ^{11}Li projectile. Furthermore, a very long-range absorption is needed to reproduce the large interaction cross section in this latter case.

In this paper, we shall present first an optical model analysis of ^{11}C elastic scattering from a ^{12}C target of the data of Ref. [4], which can be well reproduced with a standard volume Woods-Saxon potential shape for the real as well as for the imaginary part.

Second, we shall present an optical-model analysis of the ^{11}Li elastic scattering from a ^{12}C target. The data of Ref. [4] can be fitted successfully only by adding to the usual volume potential a surface term for the real and the imaginary parts. This surface term is the usual derivative of a Woods-Saxon shape. A Fuller decomposition [5] of the elastic cross section into far- and near-side components will be presented. A comparison of the two extreme isobar systems, one neutron poor, the other neutron rich, will be made.

II. THE ^{11}C ON ^{12}C ELASTIC SCATTERING ANALYSIS

Because of the poor experimental energy resolution, inelastic cross sections to the first 2^+ and the first 3^- states of ^{12}C are not separated from the pure elastic cross section. Using the automatic search code ECIS88 of Raynal [6], it has been possible to fit this global elastic cross section by calculating the distorted-wave Born approximation (DWBA) cross sections to the 4.439 MeV 2^+ and 9.641 MeV 3^- of ^{12}C and by adding them to the ground-state (g.s.) elastic cross section before computing the χ^2 value used by the automatic search routine. It is well known that in the case of heavy-ion scattering the DWBA reproduces rather well the inelastic scattering data in shape and magnitude [7]. The deformation parameters β_2 and β_3 are 0.592 and 0.400, respectively, coming from Refs. [8,9].

Figure 1 presents the global elastic scattering fit of the ^{11}C on ^{12}C data using pure volume Woods-Saxon shapes for both real and imaginary potentials. The corresponding optical-model parameters are given in Table I, family V1. The radii for real and imaginary parts are almost equal. On the other hand, the real potential has a long tail as compared to the imaginary one. This behavior is

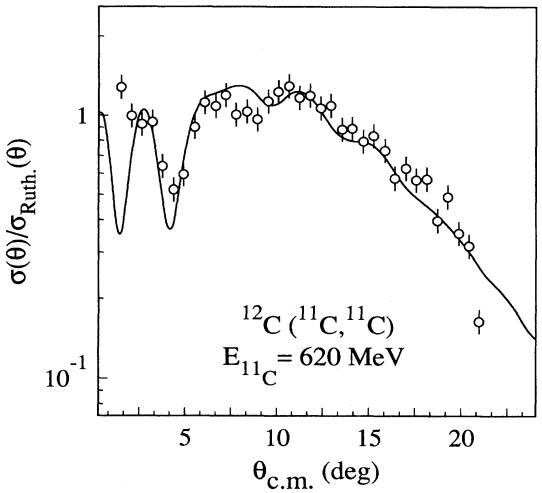

FIG. 1. Experimental angular distribution of the summed cross sections for ^{11}C elastic scattering and inelastic scatterings to the first 2^+ and 3^- states of the ^{12}C target [4]. The solid line is the result of an optical model plus DWBA fit corresponding to family V1 of Table I.

directly responsible for a strong refractive phenomenon. This kind of potential has been called in the past a surface transparent potential, since the scattered particle feels more the real part than the imaginary part of the potential, responsible mainly for diffraction. Deeper potentials produce equally good fits but with smaller radii due to the well known Igo ambiguity [10] which tells us that the elastic-scattering angular distribution is sensitive only to the tail of the optical potential. The most forward point, which deviates strongly from the Rutherford law, is not reproduced and is probably due to an experimental error. For a standard error bar of 10%, the general agreement is rather good with a χ^2 per point value of 2.4. The reaction cross section is 800.6 mb.

In Fig. 2 are presented the 2^+ and 3^- inelastic cross sections along with the ground-state elastic cross section. The sum of these three curves given in Fig. 1 reproduces the experimental data. We can see that below 8° the pure elastic scattering dominates. The oscillations of the angular distribution of the 2^+ state are out of phase with respect to the oscillations of the elastic-scattering angular distribution at backward angles. On the other hand, the 3^- oscillations look more in phase with the elastic ones. As a consequence, the pattern of the global cross section is rather unstructured at backward angles.

A decomposition into far- and near-side cross sections has been performed with the code POISON of Plagnol [11] using the formalism of Fuller [5]. Figure 3 presents the result of such decomposition. We can see that the strong forward oscillations in the elastic-scattering angular distribution are due to the "Fraunhöfer crossover" between the near- and far-side components of the elastic scattering. We can see that at backward angles after 5° the elastic angular distribution is far-side dominated with no Airy minima [14] for the far-side component. The weak oscillations seen in the elastic-scattering curve are due to the interference between the far- and near-side scattering amplitudes. Only accurate measurements with very good energy resolution would be able to pin down this oscillatory behavior and consequently to determine exactly the pattern of the near-side component at backward angles.

From the knowledge of the reaction cross section, presently 800.6 mb, it is possible to determine the strong absorption radius R from the following formulas [12] which lead to a second degree equation in R:

TABLE I. Optical-model parameter table for ^{11}C and ^{11}Li projectiles on a ^{12}C target. The χ^2 per point values correspond to standard error bars of 10%. The Coulomb radius is equal to the radius of the real part of the Woods-Saxon potential.

Projectile	^{11}C	^{11}Li	^{11}Li
E_{lab} (MeV)	620.0	637.0	637.0
Potential family	V1	V2	VS1
V (MeV)	40.0	40.0	40.0
r_0 (fm)	0.990	0.810	1.015
a_0 (fm)	0.981	1.907	1.055
W (MeV)	25.92	25.09	20.73
r_i (fm)	0.986	1.226	1.077
a_i (fm)	0.407	0.396	0.457
V_s (MeV)			2.26
r_{0s} (fm)			1.950
a_{0s} (fm)			1.201
W_s (MeV)			1.18
r_{is} (fm)			1.646
a_{is} (fm)			0.544
σ_R (mb)	800.6	1180.8	1248.0
σ_{2^+} (mb)	36.6	31.3	36.7
σ_{3^-} (mb)	13.0	11.0	13.2
χ^2	2.4	9.9	2.0

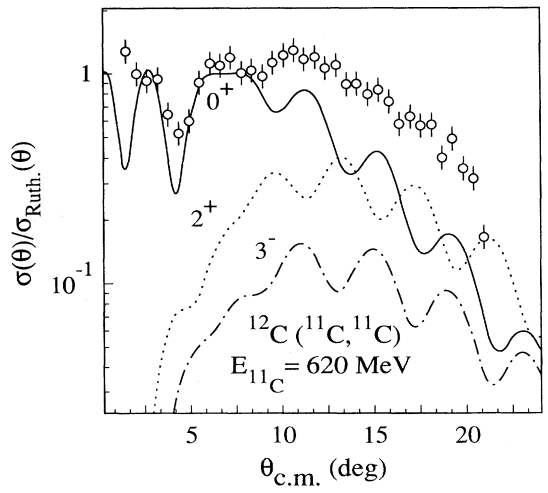

FIG. 2. Optical-model elastic, and DWBA inelastic, angular distributions of the ^{11}C projectile on the ^{12}C target. At forward angles, the elastic scattering dominates alone and fits the experimental points. The sum of these three curves is the one of Fig. 1.

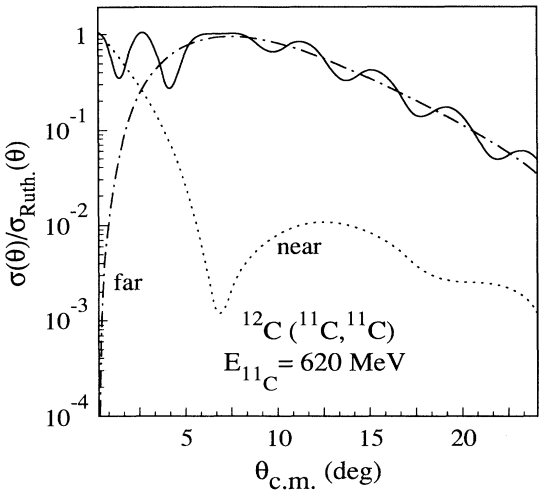

FIG. 3. Decomposition into far- and near-side components of the elastic cross section, oscillatory curve on the top of the figure, following the formalism of Fuller.

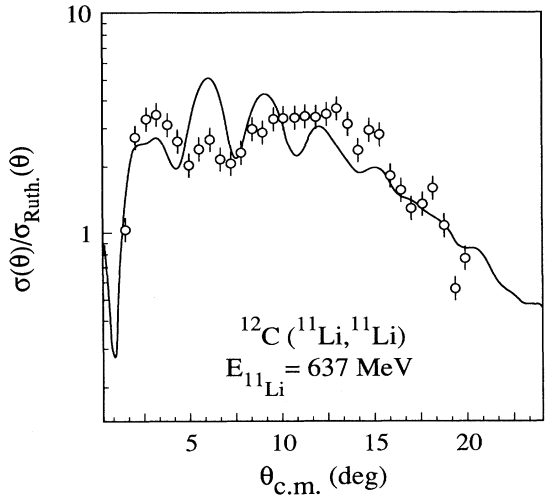

FIG. 4. Experimental angular distribution of the summed cross section for ^{11}Li elastic scattering and inelastic scatterings to the first 2^+ and 3^- states of the ^{12}C target [4]. The solid line is the result of an optical model plus DWBA fit corresponding to family V2 of Table I.

$$\sigma_R = \pi R^2 \left[1 - \frac{V_C}{E_{\text{c.m.}}} \right] ,$$

where σ_R is the reaction cross section in fm^2, $E_{\text{c.m.}}$ the center-of-mass energy, and V_C the height of the Coulomb barrier given by

$$V_C = 1.44 \frac{zZ}{R} ,$$

where z and Z are the projectile and target charges, respectively.

The strong absorption radius is 5.13 fm leading to a radius of 2.52 fm for ^{11}C and 2.60 fm for ^{12}C assuming the same $r_0 A^{1/3}$ dependence. This ^{12}C radius can be compared with the 2.472 fm value of the root-mean-square radius of the electron scattering [13]. All these results can be satisfactorily compared with the ^{12}C on ^{12}C elastic-scattering optical-model analysis performed at 1016 MeV laboratory incident energy [15].

III. THE ANALYSIS OF ^{11}Li ON ^{12}C ELASTIC SCATTERING

We present first the same kind of analysis as previously used, a volume Woods-Saxon potential. The ^{11}Li has no bound collective state and, consequently, the fact that we are considering only excitations of the ^{12}C to its first 2^+ and 3^- states is a better approximation than in case of ^{11}C on ^{12}C scattering where mutual excitations were possible. Figure 4 presents the best fit of the ^{11}Li on ^{12}C global elastic-scattering angular distribution. The quality of the fit at the forward angle is rather poor; the χ^2 per point for a standard 10% error bar is 9.9. From Table I, potential family V2, we can see that the diffusivity of the real part is very large, 1.907 fm, inducing a very long tail responsible for refractive phenomena. The absorption is also peaked quite outside the nucleus due also to the halo nature of the ^{11}Li nucleus. The oscillatory and sophisticated experimental pattern seen at forward angles below 10° is due to the interplay between diffractive and refractive phenomena [16]. A Fuller decomposition of the elastic cross section into far- and near-side components shows that the elastic scattering is dominated by the far-side amplitude at backward angles. The defect of this family is to produce at backward angles too strongly oscillating patterns in the elastic, and inelastic, angular distributions. The reaction cross section is 1180.8 mb, much larger than in the case of the ^{11}C projectile, inducing a large radius for the ^{11}Li nucleus.

In order to reproduce the experimental data at forward angles, below 8° we have used, in addition to the volume part, a surface potential for the real as well as for the imaginary part. The surface imaginary part alone does not improve the quality of the fit. The surface potential is the normalized derivative of a Woods-Saxon shape given by

$$V_s(r) = \frac{4 a_{0s} V_{0s} \exp\left[\dfrac{r - R_{0s}}{a_{0s}} \right]}{\left[1 + \exp\left[\dfrac{r - R_{0s}}{a_{0s}} \right] \right]^2}$$

with obvious notation and a similar formula for the surface imaginary part $W_s(r)$.

Figure 5 presents the best fit, strikingly good, of the global elastic scattering using the volume plus surface potential, 12 parameters, displayed in Table I, on the family name VS1. The reaction cross-section value is 1248.0 mb. The χ^2 per point value is 2.0 and the forward angles are well reproduced by the surface potential compatible with the existence of a halo for the ^{11}Li nucleus. In Fig. 6 are presented the three contributions to this global elastic

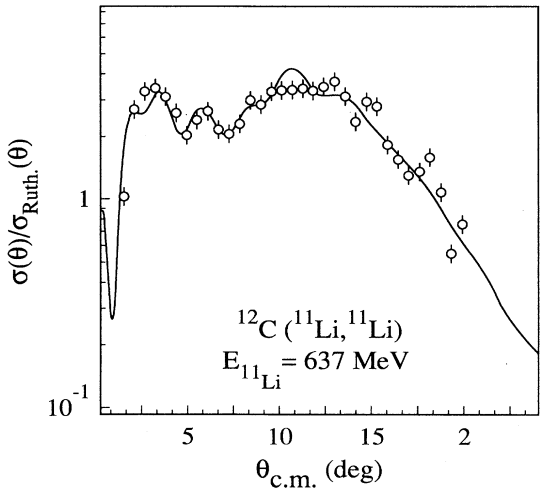

FIG. 5. Experimental angular distribution of the ^{11}Li elastic and inelastic scatterings to the first 2^+ and 3^- states of the ^{12}C target. The solid line is the result of an optical model plus DWBA fit corresponding to the volume term plus surface term family VS1 of Table I.

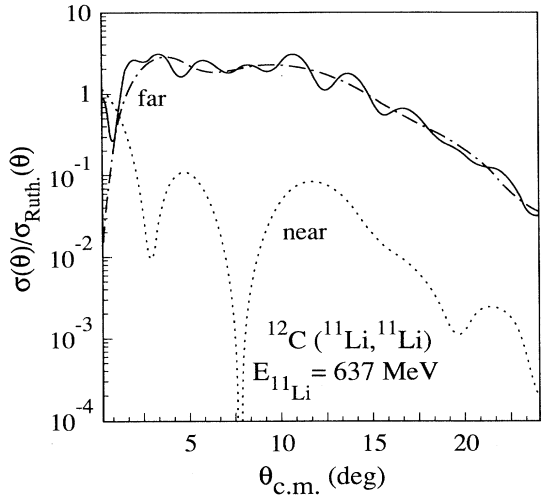

FIG. 7. Decomposition into far- and near-side components of the elastic cross section, oscillatory curve on the top of the figure, following the formalism of Fuller.

cross section along with the experimental points. We can see that at forward angles below 8° the pure elastic scattering dominates. The sum of these three curves is the calculated angular distribution of the previous Fig. 5. The decomposition of the elastic cross section into far- and near-side components is given in Fig. 7 along with the resultant elastic-scattering angular distribution. The far-side amplitude dominates and a shallow Airy minimum can be viewed in the far-side cross section at 7.5° due to the refractive effect of the real part of the surface potential. At the same angle the near-side cross section shows a deep minimum. Another way to look at the interplay between refraction and diffraction is to visualize the modulus of the S_1 matrix elements along with the deflection function, equal to twice the derivative of the Coulomb plus nuclear phase shift. This is presented in Fig. 8 where the deflection function exhibits a strong negative minimum, far-side scattering, of $-5.9°$ for a partial-wave angular momentum of $38\hbar$. A kink is also present in the $|S_1|$ matrix elements around $68\hbar$.

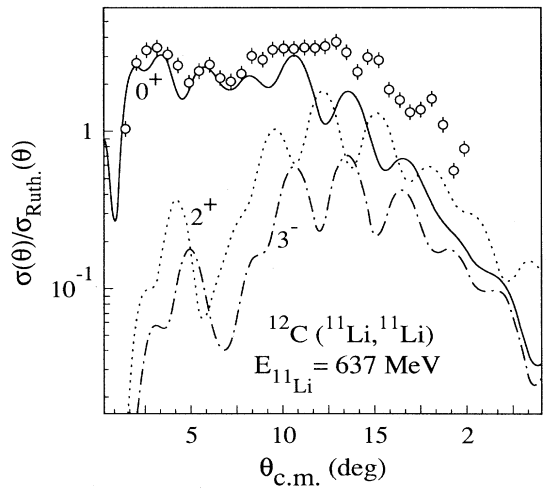

FIG. 6. Optical-model elastic, and DWBA inelastic, angular distributions of the ^{11}Li projectile on the ^{12}C target. At forward angles, the elastic scattering dominates alone and fits the experimental points. The sum of these three curves is the one of Fig. 5.

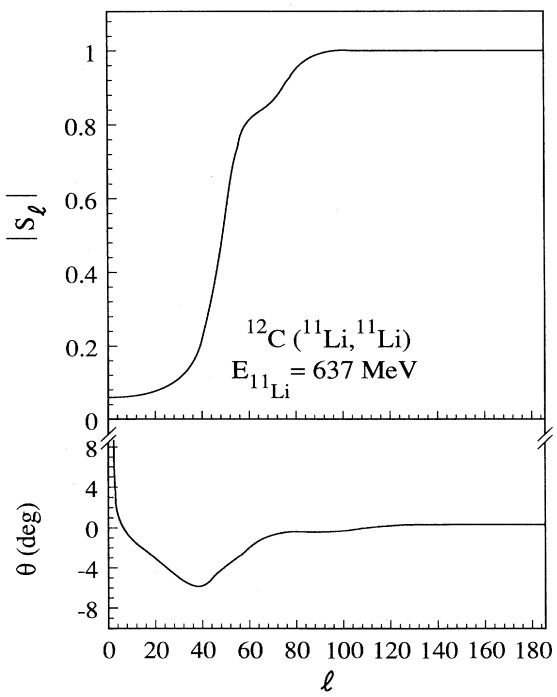

FIG. 8. The modulus of S_1 matrix elements along with the deflection function θ_1 for the ^{11}Li on the ^{12}C elastic scattering.

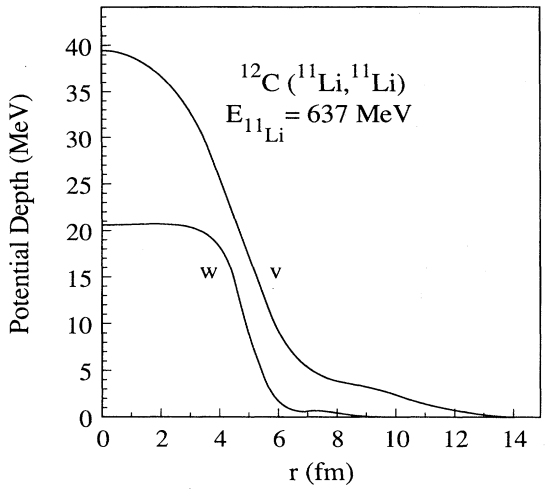

FIG. 9. Real V and imaginary W part of an optical-model potential: volume term plus surface family VS1 of Table I. The presence of a halo is evident in the real part. Furthermore, the optical potential is dramatically surface transparent.

The real and imaginary potentials are plotted in Fig. 9. The real potential exhibits a very long tail up to 12 fm due to the two-neutron halo of ^{11}Li nucleus. On the other hand, the imaginary tail is much shorter making this potential dramatically surface transparent and then very refractive. This situation is completely enhanced with respect to what is observed for ^{11}C elastic scattering in the same incident energy range. Using the same formulas for the reaction cross section than previously for the ^{11}C projectile and using the ^{12}C radius previously determined, we have found a ^{11}Li radius value of 3.74 fm corresponding to a reduced radius value of 1.68 fm. This radius value is higher than the one, 3.14 fm, determined by Tanihata *et al.* at 790 MeV/nucleon [1].

IV. CONCLUSION

It has turned out for the ^{11}Li nucleus that the observed halo increases largely the mean radius of the reaction cross section in agreement with direct reaction cross-section measurement [1] and theoretical prediction [2]. This halo gives rise to a strong refractive phenomenon never seen so clearly before for heavy-ion elastic scattering. It would be of great interest to repeat this experiment with a very good energy resolution, in order to measure separately elastic and inelastic cross sections. Refractive phenomena are already present in the ^{11}C projectile scattered by the ^{12}C target experiment, due to the presence of a surface transparent potential.

ACKNOWLEDGMENTS

Sincere thanks are due to Professor James J. Kolata of the University of Notre Dame for having provided us with his beautiful data on scattering of exotic nuclei, in tabulated form. It is also a pleasure to thank Professor Jacques Raynal from the Centre d'Etudes de Saclay for his help concerning his code ECIS88.

[1] I. Tanihata, H. Hamagaki, O. Hashimoto, Y. Shida, N. Yoshikawa, K. Sugimoto, O. Yamakawa, T. Kobayashi, and N. Takahashi, Phys. Rev. Lett. **55**, 2676 (1985).
[2] G. F. Bertsch, B. A. Brown, and H. Sagawa, Phys. Rev. C **39**, 1154 (1989).
[3] G. R. Satchler, K. W. McVoy, and M. S. Hussein, Nucl. Phys. **A522**, 621 (1991).
[4] J. J. Kolata, M. Zahar, R. Smith, K. Lamkin, M. Belbot, R. Tighe, B. M. Sherrill, N. A. Orr, J. S. Winfield, J. A. Winger, S. J. Yennello, G. R. Satchler, and A. H. Wuosmaa, Phys. Rev. Lett. **69**, 2631 (1992).
[5] R. C. Fuller, Phys. Rev. C **12**, 1561 (1975).
[6] J. Raynal, in *Applied Nuclear Theory and Nuclear Model Calculations for Nuclear Technology Applications,* Proceedings of the Workshop, Trieste, Italy, 1988, edited by M. K. Mehta and J. J. Schmidt (World Scientific, Singapore, 1988), p. 506.
[7] P. E. Hodgson, *Nuclear Heavy-Ion Reactions* (Clarendon, Oxford, 1978), p. 260.
[8] S. Raman, C. H. Malarkey, W. T. Milner, C. W. Nestor, Jr., and P. H. Stelson, At. Data Nucl. Data Tables **36**, 19 (1987).
[9] R. H. Spear, At. Data Nucl. Data Tables **42**, 81 (1989).
[10] G. Igo, Phys. Rev. Lett. **1**, 72 (1958); Phys. Rev. **117**, 1665 (1959).
[11] E. Plagnol, FORTRAN code POISON, Institut Physique de Nucléaire d'Orsay report, 1982 (unpublished).
[12] Reiner Bass, *Nuclear Reactions with Heavy Ions, TMP* (Springer, Berlin, 1980), p. 15.
[13] H. De Vries, C. W. De Jager, and C. De Vries, At. Data Nucl. Data Tables **36**, 503 (1987).
[14] Roger G. Newton, *Scattering Theory of Waves and Particles, TMP* (Springer, New York, 1982), pp. 78 and 597.
[15] M. Buenerd, A. Lounis, J. Chauvin, D. Lebrun, P. Martin, G. Duhamel, J. C. Gondrand, and P. De Saintignon, Nucl. Phys. **A424**, 313 (1984); M. C. Mermaz, B. Bonin, M. Buenerd, and J. Y. Hostachy, Phys. Rev. C **34**, 1988 (1986).
[16] M. S. Hussein and K. W. McVoy, in *Progress in Particle and Nuclear Physics,* edited by Sir Denys Wilkinson, F. R. S. (Pergamon, Oxford, 1984), Vol. 12, p. 103; K. W. McVoy and G. R. Satchler, Nucl. Phys. **A417**, 157 (1984).